

Plastic deformation mechanism of γ-phase U-Mo alloy studied by molecular dynamics simulations

Wang Chang(王畅), Peng Peng(彭芃), and Lai-Wen Sheng(赖文生)

Citation: Chin. Phys. B, 2025, 34 (**1**): 018101. DOI: 10.1088/1674-1056/ad925e

What follows is a list of articles you may be interested in

Unravelling biotoxicity of graphdiyne: Molecular dynamics simulation of the interaction between villin headpiece protein and graphdiyne

Bei-Wei Zhang(张贝薇), Bing-Quan Zhang(张兵权), Zhi-Gang Shao(邵志刚), and Xianqiu Wu(吴先球)
Chin. Phys. B, 2024, 33 (**11**): 118102. DOI: 10.1088/1674-1056/ad7af5

Molecular dynamics study of thermal conductivities of cubic diamond, lonsdaleite, and nanotwinned diamond via machine-learned potential

Jia-Hao Xiong(熊佳豪), Zi-Jun Qi(戚梓俊), Kang Liang(梁康), Xiang Sun(孙祥), Zhan-Peng Sun(孙展鹏), Qi-Jun Wang(汪启军), Li-Wei Chen(陈黎玮), Gai Wu(吴改), and Wei Shen(沈威)
Chin. Phys. B, 2023, 32 (**12**): 128101. DOI: 10.1088/1674-1056/ace4b4

Thermal and mechanical properties and micro-mechanism of SiO_2/epoxy nanodielectrics

Tian-Yu Wang(王天宇), Gui-Xin Zhang(张贵新), and Da-Yu Li(李大雨)
Chin. Phys. B, 2021, 30 (**12**): 128101. DOI: 10.1088/1674-1056/abff2c

Prediction of structured void-containing 1T-$PtTe_2$ monolayer with potential catalytic activity for hydrogen evolution reaction

Bao Lei(雷宝), Yu-Yang Zhang(张余洋), Shi-Xuan Du(杜世萱)
Chin. Phys. B, 2020, 29 (**5**): 058104. DOI: 10.1088/1674-1056/ab8203

Density functional calculations of efficient H_2 separation from impurity gases (H_2, N_2, H_2O, CO, Cl_2, and CH_4) via bilayer g-C_3N_4 membrane

Yuan Guo(郭源), Chunmei Tang(唐春梅), Xinbo Wang(王鑫波), Cheng Wang(王成), Ling Fu(付玲)
Chin. Phys. B, 2019, 28 (**4**): 048102. DOI: 10.1088/1674-1056/28/4/048102

Plastic deformation mechanism of γ-phase U–Mo alloy studied by molecular dynamics simulations

Chang Wang(王畅), Peng Peng(彭芃), and Wen-Sheng Lai(赖文生)†

The Key Laboratory of Advanced Materials (MOE), School of Materials Science and Engineering, Tsinghua University, Beijing 100084, *China*

(Received 25 July 2024; revised manuscript received 19 September 2024; accepted manuscript online 14 November 2024)

Uranium–molybdenum (U–Mo) alloys are critical for nuclear power generation and propulsion because of their superior thermal conductivity, irradiation stability, and anti-swelling properties. This study explores the plastic deformation mechanisms of γ-phase U–Mo alloys using molecular dynamics (MD) simulations. In the slip model, the generalized stacking fault energy (GSFE) and the modified Peierls–Nabarro (P–N) model are used to determine the competitive relationships among different slip systems. In the twinning model, the generalized plane fault energy (GPFE) is assessed to evaluate the competition between slip and twinning. The findings reveal that among the three slip systems, the $\{110\}\langle 111\rangle$ slip system is preferentially activated, while in the $\{112\}\langle 111\rangle$ system, twinning is favored over slip, as confirmed by MD tensile simulations conducted in various directions. Additionally, the impact of Mo content on deformation behavior is emphasized. Insights are provided for optimizing process conditions to avoid $\gamma \rightarrow \alpha''$ transitions, thereby maintaining a higher proportion of γ-phase U–Mo alloys for practical applications.

Keywords: U–Mo alloy, molecular dynamics simulation, plastic deformation mechanism, dislocation slip, twin formation

PACS: 81.05.Bx, 31.15.xv, 81.40.Lm, 61.72.Lk, 61.72.Mm

DOI: 10.1088/1674-1056/ad925e **CSTR:** 32038.14.CPB.ad925e

1. Introduction

Uranium (U) alloys are essential in key areas such as nuclear power generation and nuclear propulsion.[1] The swelling behavior induced by irradiation in metallic nuclear fuels under high-temperature and irradiation conditions can present significant safety hazards.[2] γ-phase U-based metallic nuclear fuels are regarded as advanced nuclear fuels due to their thermal conductivity, performance under irradiation, and resistance to swelling.[3] Recently, uranium–molybdenum (U–Mo) alloys have emerged as promising fuel candidates for fast neutron breeder reactors because of their outstanding irradiation stability, high density, fissile characteristics, high thermal conductivity, and low production costs.[2] Extensive investigations have been conducted on their mechanical properties,[8] phase stability,[4] and phase transformations,[12] revealing that the incorporation of Mo effectively stabilizes the γ-phase, thereby improving its thermal conductivity and anti-swelling capabilities.[14]

The ground-state structure of U-based alloys is the low-symmetry orthorhombic α-phase. Currently, there is abundant research on the mechanical properties of α-phase U-based alloys, especially the mechanisms of plastic deformation.[15] However, the practical demand for nuclear fuel now tends toward γ-phase U-based alloys with superior comprehensive properties. Therefore, this study focuses on exploring the mechanical properties of γ-phase U–Mo alloys from a plasticity perspective. Slip is generally the primary mechanism responsible for the plastic deformation of metallic materials, while other deformation modes, such as twinning and kinking, act as supplementary mechanisms under certain thermodynamic conditions and loading scenarios where slip is challenging to attain. In the case of U-based alloys, the intricate electronic structure results in asymmetry within their structure and deformation modes. In the analysis of plastic deformation, regardless of whether in the α- or γ-phases, twinning deformation consistently plays a significant role.

This study employs molecular dynamics (MD) simulation methods to explore the plastic deformation mechanisms of γ-phase U–Mo alloys. By constructing slip models and solving the generalized stacking fault energy (GSFE) and modified Peierls–Nabarro (P–N) models, we investigate the preferentially activated slip system. We have refined the form of the restoring force in the P–N model, so it is no longer fixed as the traditional sine function is, making our model more representative of actual conditions. Unlike previous mechanical studies, which have focused primarily on the macroscopic mechanical properties and defect behaviors under specific conditions, the present study focuses on the micro-level analysis of slip and twinning competing mechanisms, which is crucial for understanding the deformation behavior of alloys in practical applications. By constructing twinning models and solving the generalized plane fault energy (GPFE), we explore the preferentially activated twinning system. Finally, to validate the above findings, we performed molecular dynamic tensile

†Corresponding author. E-mail: wslai@tsinghua.edu.cn

© 2025 Chinese Physical Society and IOP Publishing Ltd. All rights, including for text and data mining, AI training, and similar technologies, are reserved.

simulations along different crystalline directions and determined which tensile direction favored $\gamma \rightarrow \alpha''$ phase transformations. Understanding the plastic deformation mechanisms of γ phase U–Mo alloys will provide useful guidance for the actual processing of alloys so that the selected processing will favor twinning and inhibit phase transformations to maintain a greater proportion of the γ phase in metallic U–Mo fuels.

2. Simulation methods

The occurrence of slip and twinning is contingent upon the movement of dislocations within the system. Building on prior studies,[17] Ojha *et al.*[20] explored BCC-type Fe-based alloys by generating dislocations through rigid translation and subsequently developing slip and twinning models. Microscopic deformation processes were simulated to obtain the GSFE and GPFE, which closely align with experimental values, thereby effectively validating the applicability of these theories for determining plastic deformation mechanisms. The calculation formulas for GSFE and GPFE are as follows:

$$\gamma = (E_{\mathrm{s}} - E_0)/(2A), \tag{1}$$

where γ represents the crystal's generalized fault energy, E_{s} and E_0 are the energies of the deformed crystal and the perfect crystal, respectively, and A is the area of the deformation plane. A factor of 2 is ascribed to two slip or twin planes existing in the system owing to the application of the periodic boundary conditions in all directions.

The P–N model is a fundamental concept in dislocation theory.[21] The Peierls stress (τ_{p}) represents the shear stress necessary to initiate dislocation slip and serves as the resistance to dislocation motion, which is influenced by the misfit between atomic planes. In conventional calculations of Peierls stress, the restoring force in materials is typically assumed to be a sinusoidal function, which does not accurately reflect real conditions. Therefore, the form of the restoring force is improved by analyzing the GSFE curve, eliminating the reliance on a fixed sinusoidal model. The GSFE curve is derived through rigid displacement, where the atomic arrangements above and below the slip plane are uniform; thus, the restoring force can be expressed as the first derivative of the GSFE with respect to displacement u, satisfying the relation

$$f_{xy} = -\mathrm{d}\gamma/\mathrm{d}u. \tag{2}$$

The self-consistent method is then employed to resolve and obtain the Peierls stress. This modified approach brings the calculations closer to actual material deformation, although it has several limitations. Firstly, since the restoring force is regarded as the first derivative of the GSFE with respect to displacement, the accuracy of the GSFE directly influences the model's precision. The calculation of the GSFE is affected by the construction of the slip model and the accuracy of the potential function used, which can lead to errors in determining misfit energy and Peierls force. Secondly, the P–N model is fundamentally a zero-temperature model, while the deformation behavior of materials can vary significantly at elevated temperatures. Neglecting temperature effects may restrict the model's applicability under high-temperature conditions. Additionally, the model typically assumes uniaxial stress conditions for the analysis of dislocation slip, yet in practical applications, materials are often subjected to complex multiaxial stress states, which can impact dislocation movement mechanisms.

Previous studies have shown[25] that U–Mo alloys form a stable γ-phase when the Mo content is greater than 14 at.%, so the compositions of the models in this study are U–15 at.% Mo (U–6.64 wt.% Mo), U–20 at.% Mo (U–8.66 wt.% Mo), and U–25 at.% Mo (U–10.60 wt.% Mo). Owing to the large-scale system calculations that are possible with the MD method, we construct U–Mo random solid solutions with different compositions through random doping, which better match the disordered state in real U–Mo alloys. Notably, GSFEs focus primarily on defects near the fault plane, so when doping atoms, it is necessary to divide the entire simulation box into different atomic layers and dope near the fault plane and other locations separately. This will ensure accurate doping of the atom content near the fault plane, thus avoiding size effects.

When plane defects are established through rigid translation, the boundary conditions of the model are periodic. If the fault plane is not aligned with the axial plane of the unit cell (i.e., $xoy/xoz/yoz$ plane), the periodicity at the boundaries of the unit cell will result in atomic misalignment, which disrupts the calculation outcomes. Consequently, a coordinate system transformation is conducted, positioning the fault plane as the xoy plane, with the atoms in the system receiving new coordinates based on this updated base plane. The specific approach entails utilizing MATLAB to compute the transformation matrix based on the coordinate transformation relation provided in Eq. (3), followed by substituting the coordinates of the crystal in the general axial plane, x_i, into the equation to derive the new coordinates, x_i', as shown below:

$$[x_i'] = \begin{bmatrix} x_1' \\ x_2' \\ x_3' \end{bmatrix} = \begin{bmatrix} a_{11} & a_{12} & a_{13} \\ a_{21} & a_{22} & a_{23} \\ a_{31} & a_{32} & a_{33} \end{bmatrix} \begin{bmatrix} x_1 \\ x_2 \\ x_3 \end{bmatrix}. \tag{3}$$

We take the $\{112\}\langle 111\rangle$ slip system of the γ-phase U–15 at.% Mo alloy as an example to elaborate on the construction process of the random solid solution. The orientation of the twinning model aligns with the $\{112\}\langle 111\rangle$ system in the slip model. First, the (112) plane is identified as the xoy plane of the unit cell, and the slip direction $[11\bar{1}]$ is designated the y-axis direction to avoid the influence of periodic boundary

conditions. The unit cell is subsequently expanded by a factor of 50 in the x, y and z directions, resulting in a supercell of pure γ-phase U consisting of 300 layers and a total of 750000 atoms. This substantial atom count enables the model to effectively simulate real conditions. Next, Mo atoms are introduced into the supercell. With the slip plane serving as the symmetry plane, the entire unit cell is divided into two relatively uniform layers above and below this plane. The U atoms in the four layers situated above and below the slip plane are randomly substituted with 15 at.% Mo atoms, while the remaining atoms outside these eight layers are uniformly replaced. This approach guarantees that the appropriate proportion of Mo atoms influences the fault energy, thus mitigating size effects. The same procedure is applied to adjust the Mo atomic proportion to 20 at.% and 25 at.% in order to create slip models for the other two compositions of the $\{112\}\langle111\rangle$ system. Similarly, by altering the *xoy* plane to other slip planes, slip models for the $\{110\}\langle111\rangle$ and $\{123\}\langle111\rangle$ systems can be developed.

To achieve high computational accuracy in MD simulations, understanding atomic interactions, specifically the potential function, is essential. The angle-dependent potential (ADP) introduced by Starikov in 2017[26] is employed to simulate the microscopic plastic deformation mechanisms of γ-phase U–Mo alloys. The complexity of the ADP is intermediate between that of the embedded atomic method (EAM) potential and the modified EAM (MEAM) potential. It offers high computational accuracy and broad applicability, demonstrating notable advantages in computational efficiency compared to the MEAM potential, and is extensively utilized in multibody system simulations. The ADP function is particularly suitable for materials like U–Mo alloys, which exhibit complex phase transition behaviors, as it incorporates the angular dependence between atoms. The referenced literature highlights that this potential function is specifically designed to describe γ-phase U–Mo alloys and their metastable phases (such as γ' and other distorted lattice structures), as well as the mechanical properties of the alloy, including elastic moduli and phase transition temperatures.

3. Slip model

3.1. GSFE

Using the $\{112\}\langle111\rangle$ system as an example, the process for obtaining the GSFE curve is described. Following the establishment of the slip model, the entire simulation box is divided into two regions, with the slip plane acting as the symmetry plane. The upper region is displaced along the slip direction by an increment of $\boldsymbol{b}/30$ for a total of 30 displacements, resulting in the upper region being displaced by $\boldsymbol{b}$ relative to the lower region. For the three slip systems, the slip direction is $\langle111\rangle$, and $\boldsymbol{b}$ represents the Burgers vector of $(\boldsymbol{a}/2)[111]$, where $\boldsymbol{a}$ is the lattice constant of the γ-phase U–Mo alloy. To ensure accuracy in energy calculations and to prevent atomic loss, atoms are permitted to move freely along the z-axis. After each displacement, the energy of the stabilized crystal is computed and recorded, yielding the GSFE curve illustrated in Fig. 1. Additionally, the energy barriers, $\gamma_{\mathrm{us}}^{\mathrm{slip}}$, that must be surpassed for slip in the three slip systems are presented in Table 1.

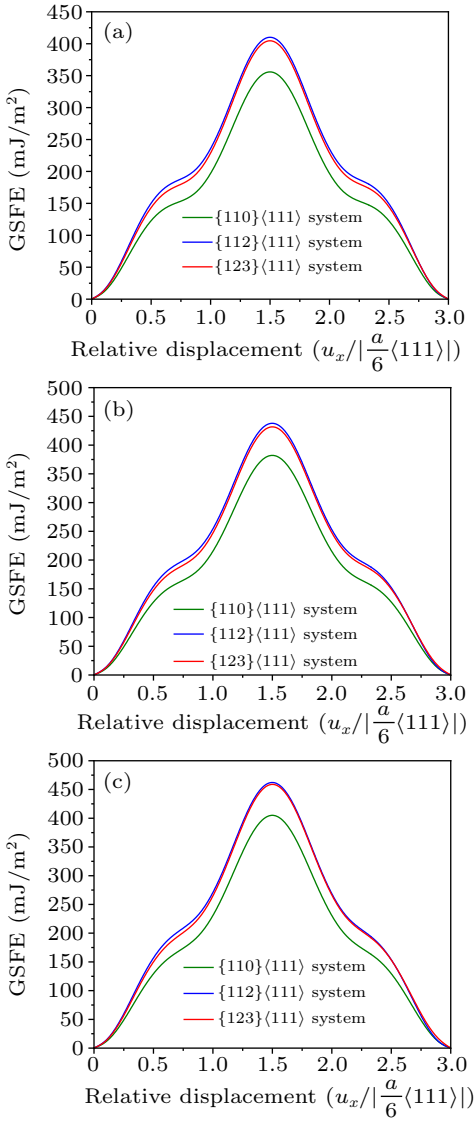


Fig. 1. GSFE curves of three slip systems for U–Mo alloys of (a) U–15 at.% Mo, (b) U–20 at.% Mo, and (c) U–25 at.% Mo.

Figure 1 and Table 1 show that for the same slip system, the energy barrier increases with increasing Mo content. However, the Mo content does not affect the relative order of the energy barriers for the three slip systems, with the $\{110\}\langle111\rangle$ system having the lowest values and the $\{112\}\langle111\rangle$ system having the highest energy barriers. We preliminarily conclude that the $\{110\}\langle111\rangle$ slip system is the easiest to activate, but whether it is activated first depends on the orientation and direction of the external force. We further verify this conclusion

by solving the P–N model.

Table 1. Energy barriers γ_{us}^{slip} on three slip systems of different compositions of alloys.

Composition	Slip system	γ_{us}^{slip} (mJ/m^2)
U–15 at.% Mo	$\{110\}\langle111\rangle$	359.31
	$\{112\}\langle111\rangle$	413.85
	$\{123\}\langle111\rangle$	408.38
U–20 at.% Mo	$\{110\}\langle111\rangle$	385.87
	$\{112\}\langle111\rangle$	441.93
	$\{123\}\langle111\rangle$	435.75
U–25at.%Mo	$\{110\}\langle111\rangle$	409.00
	$\{112\}\langle111\rangle$	466.44
	$\{123\}\langle111\rangle$	463.16

3.2. Misfit energy and Peierls stress

We use the P–N model to further analyze the priority of slip system activation from the perspectives of misfit energy and Peierls stress. From the previous analysis of the GSFE, it is evident that an increase or decrease in Mo content does not affect the priority order of slip system activation. Therefore, all calculations in this section are illustrated using the γ-phase U–15 at.% Mo as an example.

First, we calculate the misfit energy. After the dislocation movement of $\alpha\boldsymbol{b}$, the total misfit energy is as follows:[24]

$$\varepsilon_{AB} = \sum_{n=-\infty}^{\infty} \frac{Gb^3}{4\pi^2 a} \frac{\xi^2}{[(\frac{n}{2}-\alpha)b]^2+\xi^2} = \frac{Gb^2}{4\pi(1-\nu)} + \frac{E_P}{2}\cos 4\pi\alpha, \tag{4}$$

$$E_P = \frac{Gb^2}{\pi(1-\nu)} e^{-\frac{2\pi\omega}{b}}, \tag{5}$$

where n is an integer, E_P represents the potential energy of periodic displacement, G denotes the alloy shear modulus, a indicates the distance between slip planes, and $\omega = a/(1-\nu)$ is the dislocation width (which corresponds to the distance between the two points when the displacement reaches half of the maximum displacement). Additionally, ξ represents half of the dislocation width, and ν is Poisson's ratio. The corresponding function in Fig. 2(a) shows that the energy barrier of the $\{110\}\langle111\rangle$ system is the lowest, satisfying the relationship of the energy barrier $\Delta W_{\{110\}\langle111\rangle} < \Delta W_{\{112\}\langle111\rangle} < \Delta W_{\{123\}\langle111\rangle}$.

The Peierls stress is then calculated. By differentiating the x-axis in Fig. 1(a), the restoring force f_{xy} graph depicted in Fig. 2(b) is obtained. The maximum value of the restoring force is extracted and substituted into the enhanced Peierls stress formula

$$\sigma_P = 2K\exp\left(-\frac{K}{f_{xy(\max)}}\right), \tag{6}$$

$$K = \frac{G}{1-\nu}, \tag{7}$$

$$f_{xy(\max)} = \left|\frac{d\gamma}{du}\right|_{\max}, \tag{8}$$

where G is the shear modulus and ν is the Poisson's ratio. The Peierls stresses of the $\{110\}\langle111\rangle$, $\{112\}\langle111\rangle$, and $\{123\}\langle111\rangle$ slip systems are 478.99 MPa, 1062.82 MPa, and 1533.82 MPa, respectively, satisfying the relationship of $\tau_{p,\{110\}\langle111\rangle} < \tau_{p,\{112\}\langle111\rangle} < \tau_{p,\{123\}\langle111\rangle}$.

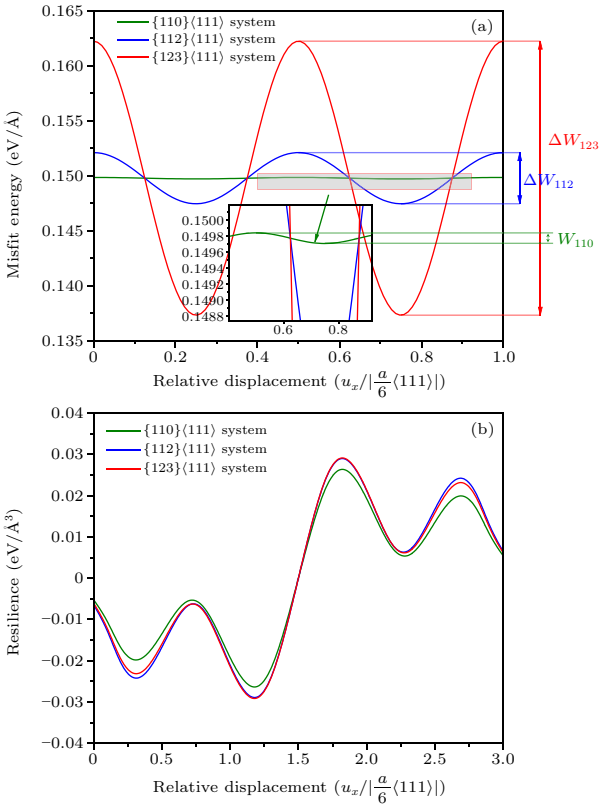


Fig. 2. (a) Misfit energies of three slip systems of U–15 at.% Mo. ΔW represents the energy barrier that each slip system needs to cross. (b) Recovery stress on three slip systems of U–15 at.% Mo.

3.3. Competition mechanism of different slip systems

Above all, from both the misfit energy and Peierls stress perspectives, we conclude that the $\{110\}\langle111\rangle$ slip system is the primary slip system and is most likely to activate first in the internal competition of slip systems. Since Fig. 1 shows that the GSFE curves for the γ-phase U–Mo alloys with three compositions are highly similar and that the relative order of the curves does not change, it can be inferred that for the γ-phase U–20 at.% Mo and U–25 at.% Mo alloys, the $\{110\}\langle111\rangle$ slip system is still most likely to be activated first. Importantly, this inference is based on the assumption that Mo is randomly distributed in the alloy. However, in practical situations, as deformation continues, Mo atoms may cluster near the dislocation core. If the clustering degree of Mo atoms near the dislocation core differs among the different slip systems, it could impact the results.

In actual material deformation experiments, the priority sequence of slip system activation must also take into account

the Schmid factor ε. Slip occurs only when the shear stress along a slip direction on a slip plane exceeds the critical resolved shear stress $\tau_{\rm crss}$. Although the Peierls stress and $\tau_{\rm crss}$ are not identical, both are associated with the onset of plastic deformation and share the same physical significance. Therefore, the ratio of Peierls stress to the Schmid factor, $\tau_{\rm p}/\varepsilon$, is utilized to determine the priority of the three slip systems, with the system having the smallest $\tau_{\rm p}/\varepsilon$ ratio being activated first.

For the $\{110\}\langle 111\rangle$ slip system, which has the smallest Peierls stress, the minimum value of the maximum Schmid factor under various loading directions is as follows:

$$\varepsilon_{\{110\}\langle 111\rangle} = \min\{\max[\varepsilon_{\{110\}\langle 111\rangle}(\boldsymbol{F})]\} = 0.2722. \quad (9)$$

For the other two systems with larger Peierls stresses, the maximum value of the Schmid factor is 0.5. To ensure the generality of the results, we take the smaller Schmid factor value for the $\{110\}\langle 111\rangle$ system in the slip hard orientation, whereas we take the maximum Schmid factor value for the other two systems in the slip soft orientation. This satisfies the following relationship:

$$\frac{\sigma_{\rm P}\{110\}\langle 111\rangle}{0.2722} < \frac{\sigma_{\rm P}\{112\}\langle 111\rangle}{0.5} < \frac{\sigma_{\rm P}\{123\}\langle 111\rangle}{0.5}. \quad (10)$$

On the basis of the current computation and simulation results, the $\{110\}\langle 111\rangle$ slip system tends to be the first to activate under certain specific loading directions, but this conclusion may vary under different material conditions (temperature, stress state, etc.). We compared these results with the experimental results of Jia Jianping *et al.*,[27] who conducted tensile tests on U–10 at.% Mo alloys at room temperature and obtained a yield strength of 870 MPa. In our study, considering both the Peierls stress and Schmid factor for U–15 at.% Mo, the yield strength should be 957.98 MPa. This calculated value is slightly greater than the experimental value, with an error of about 10%, which can be attributed to factors such as the differences in material composition (polycrystalline U–10 at.% Mo in the experiment vs. single-crystal U–15 at.% Mo in the simulation), temperature differences, and differences in dislocation motion under thermal activation. In general, the calculation results are on the same order of magnitude as the experimental yield strength, supporting the reliability of the simulations.

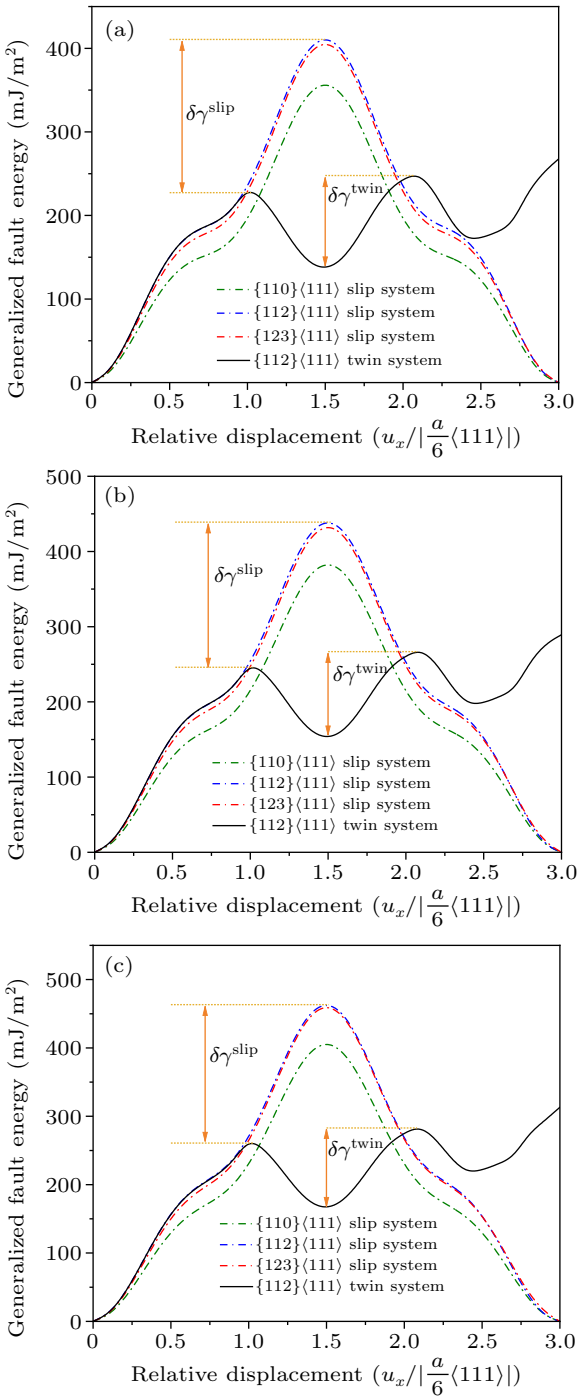


Fig. 3. Generalized fault energy curves for three slip systems of (a) U–15 at.% Mo, (b) U–20 at.% Mo, and (c) U–25 at.% Mo. $\delta\gamma^{\rm slip}$ represents the energy barrier that must be overcome to continue slipping after a $(\boldsymbol{a}/6)\langle 111\rangle$ partial dislocation is formed. $\delta\gamma^{\rm twin}$ represents the energy barrier that must be overcome to continue twinning after a $(\boldsymbol{a}/6)\langle 111\rangle$ partial dislocation is formed.

4. Twinning model

4.1. GPFE

The selection of potential functions, lattice constants, and other parameters for the twinning model, as well as the relaxation and energy output operations, are consistent with those used for the slip model. The primary distinction between the two lies in the formation of the stacking fault. In the slip model, the upper portion of the crystal is displaced as a whole in relation to the lower part along the slip plane. In constructing the twinning model with rigid shear, twins are generated by creating continuous stacking faults. Initially, the twinning planes at the center and top of the simulation box are designated as boundaries, dividing the entire simulation box into upper and lower sections. The upper section is translated 10 times relative to the lower section, with each translation distance set at $\boldsymbol{b}/30$, resulting in a total distance of $\boldsymbol{b}/3$. Subse-

quently, the twinning plane is shifted up one atomic layer in the middle and down one atomic layer at the top, establishing new boundaries and repeating the first translation operation, leading to a $\boldsymbol{b}/3$ displacement. Finally, the twinning planes are shifted up by one atomic layer in the middle and down by one atomic layer at the top to define new boundaries, and this translation operation is repeated. After completing these operations, two stable three-layer twins with a total translation distance of $\boldsymbol{b}$ are formed in the model. The energy of the stable state after each displacement is calculated and output to generate the GPFE curve. When combined with the GSFE curve from Fig. 1, the generalized fault energy for various compositions of the γ-phase U–Mo alloys is obtained, as illustrated in Fig. 3. Regardless of composition, the energy barrier for twinning is consistently lower than that for slipping. This preliminary observation indicates that twinning is likely to occur prior to slip in the $\{112\}\langle 111\rangle$ system.

4.2. Competing mechanism between slip and twinning

In the case when a $(\boldsymbol{a}/6)\langle 111\rangle$ partial dislocation forms in the system, its subsequent movement can either occur within the same $\{112\}$ plane until the displacement is large enough to cause slip, or it can move across a series of consecutive $\{112\}$ planes to result in twinning. Previous research has shown[28] that the competitive priority between slip and twinning can be determined by the ratio of $\delta\gamma^{\text{twin}}/\delta\gamma^{\text{slip}}$. A ratio of $\delta\gamma^{\text{twin}}/\delta\gamma^{\text{slip}} > 1$ favors slip, whereas a ratio < 1 favors twinning. The ratios of $\delta\gamma^{\text{twin}}/\delta\gamma^{\text{slip}}$ for the three different U–Mo alloys are given in Table 2. An analysis of the data in Table 2 reveals that $\delta\gamma^{\text{twin}}/\delta\gamma^{\text{slip}} < 1$ is valid for all three compositions of the γ-phase U–Mo alloys. This means that for the $\{112\}\langle 111\rangle$ system, twinning is likely to occur before slipping under external loading.

However, since it is not feasible to compare the priority order between the $\{110\}\langle 111\rangle$ slip system and the $\{112\}\langle 111\rangle$ twinning system through computational simulation, it cannot be concluded that twinning will necessarily occur before slip in the actual deformation of γ-phase U–Mo alloys. This process is influenced by numerous factors, including alloy composition, loading method, loading temperature, and loading orientation. Furthermore, the results presented in Table 2 indicate that as the Mo content increases, the ratio of $\delta\gamma^{\text{twin}}/\delta\gamma^{\text{slip}}$ gradually decreases, suggesting that an increase in Mo content can positively influence the occurrence of twinning.

Table 2. Determination of the ratio of $\delta\gamma^{\text{twin}}$ to $\delta\gamma^{\text{slip}}$.

Composition	$\delta\gamma^{\text{twin}}$ (mJ/m^2)	$\delta\gamma^{\text{slip}}$ (mJ/m^2)	$\delta\gamma^{\text{twin}}/\delta\gamma^{\text{slip}}$
U–15 at.% Mo	115.17	180.03	0.64
U–20 at.% Mo	118.79	189.96	0.63
U–25 at.%Mo	120.99	199.16	0.61

4.3. Tensile model

To verify the accuracy of the previously determined priorities in plastic deformation, uniform tensile simulations are conducted on γ-phase U–15 at.% Mo alloys along the [100] and [110] directions. The tensile direction is aligned with the x-axis, and strain is applied along this axis during the calculations. To enhance the precision of the results, the model is initially relaxed at a low temperature of 10 K for 10 ps to achieve the most stable energy state, followed by tensile testing at room temperature with a time step of 0.002 ps and a strain rate of 1.0×10^{9} s^{-1}. The periodic boundary condition is enforced along the tensile direction, while the free boundary condition is implemented along the other two directions.

The stress–strain variations during the tensile process are presented in Fig. 4. For tensile testing along the [100] direction, as strain increases, the stress curve can be categorized into three distinct stages: the first stage represents the elastic deformation phase, where the stress curve resembles a linear function, with the slope corresponding to the elastic modulus; the second stage indicates microplastic deformation, characterized by a notable change in the slope of the stress curve compared to the first stage, along with a decrease in flatness; the third stage marks the yield phase, during which the stress value reaches a maximum, and the curve may display yield plateaus or yield serrations, reflecting irregular wave-like patterns under rheological conditions. The stress–strain curve for tensile testing in the [110] direction exhibits some similarities but does not include the microplastic deformation stage.

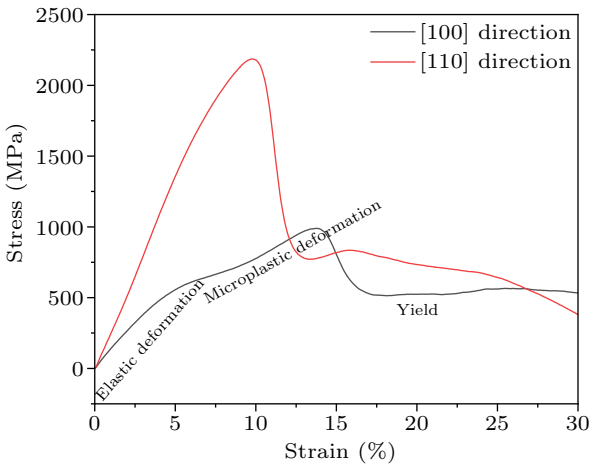


Fig. 4. Stress–strain curves for tensile testing along the [100] and [110] directions.

The stress–strain curve for the [100] direction clearly demonstrated a plastic deformation stage. Consequently, structural files for this stage were generated, revealing significant twinning. Ovito[29] software was utilized for dislocation analysis to identify the twinning planes, and the atomic coloring function was employed to indicate the twinning system. The results of the dislocation analysis are presented in

Fig. 5(a). By calculating the atomic coordinates, the twinning plane was initially identified as $(21\bar{1})$. Due to the higher energy of atoms near the twin boundary compared to other atoms, the atomic coloring function was applied to determine the shear plane and twinning direction, coloring atoms based on their energy levels. The marking results are illustrated in Fig. 5(b), where the red line represents the symmetrical partial twinning structure, with the shear plane identified as (011) and the twinning direction being $[1\bar{1}1]$. This twinning system is classified as $\{112\}\langle 111\rangle$, aligning with prior molecular statics calculations.

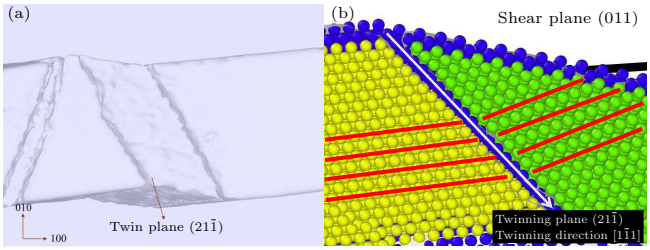


Fig. 5. (a) Defect surface grid analysis of U–15 at.% Mo, with the twinning plane determined as $(21\bar{1})$. (b) Calibration analysis of the twinning structure, with the shear plane being (011), the twinning plane being $(21\bar{1})$ and the twinning direction being $[1\bar{1}1]$.

In contrast to the tensile results along the [100] direction, no twinning configurations were observed in the tensile results along the [110] direction, and the stress–strain curve also exhibited notable differences. Initially, common neighbor analysis was conducted on the models in both directions. The results are presented in Table 3, and the corresponding atomic configuration diagrams are displayed in Figs. 6(a) and 6(b). For the [100] direction, the results indicate that the majority of atoms remain in the BCC structure, with atoms undergoing structural changes located only on the surface of the solid solution, implying that γ-phase U–Mo alloys do not experience phase transformation when subjected to tensile stress in this direction. Conversely, the results for the [110] direction reveal that about 50% of the atoms have transitioned from the BCC structure to alternative structures, with the atoms undergoing structural changes distributed throughout the solid solution, indicating that phase transformation has taken place.

To more precisely identify the phase transformation structure resulting from tensile testing along the [110] direction,

Table 3. Results of common neighbor analysis in both tensile directions.

[100] direction					
Structure	other	FCC	HCP	BCC	ICO
Count	78174	23	23	498580	0
Fraction	13.6%	0.0%	0.0%	86.4%	0.0%
[110] direction					
Structure	other	FCC	HCP	BCC	ICO
Count	572004	1923	6836	572677	0
Fraction	49.6%	0.2%	0.6%	49.6%	0.0%

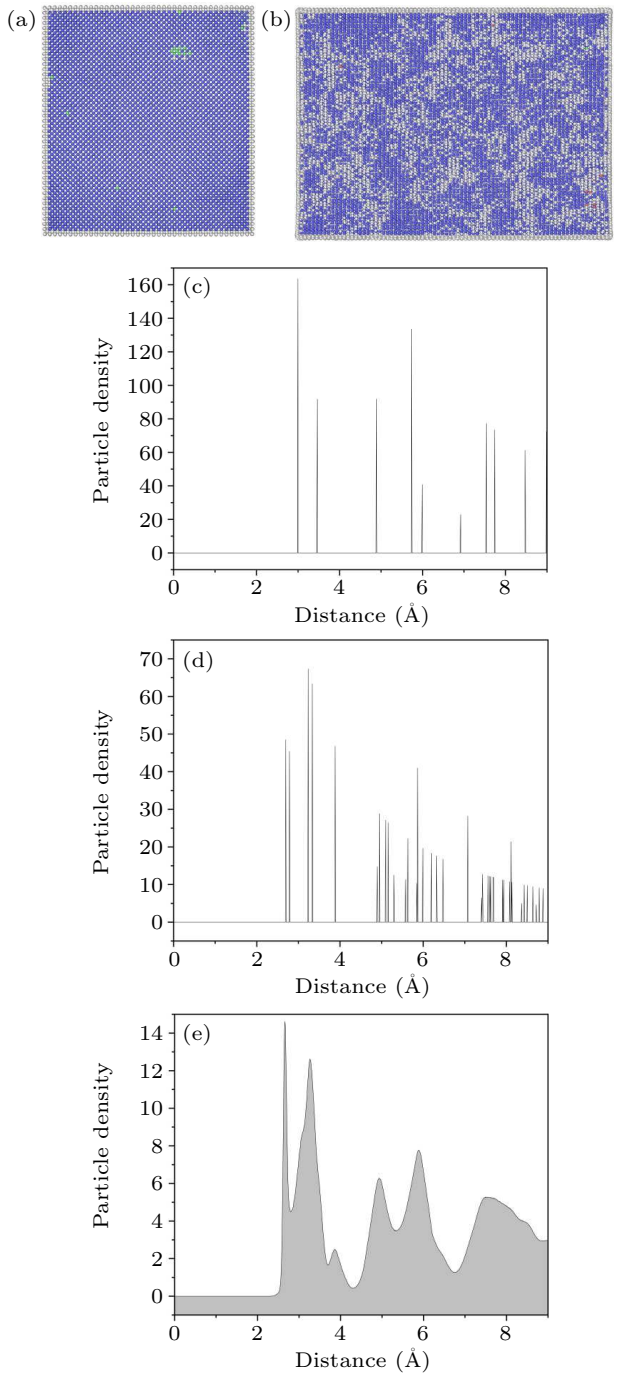


Fig. 6. Atomic configuration diagrams for tensile testing along the (a) [100] direction and (b) [110] direction, where BCC atoms are marked in blue, FCC atoms are marked in green, HCP atoms are marked in red, ICO atoms are marked in yellow, and other atoms are marked in grey; radial distribution functions of (c) the perfect BCC crystal, (d) the perfect orthorhombic crystal and (e) 8% tensile strain along the [110] direction.

the phase structure was examined using the radial distribution function (RDF). The RDFs of the structure with 8% strain along the [110] direction were compared to those of the perfect BCC crystal structure and the perfect orthorhombic crystal structure, as shown in Figs. 6(c)–6(e). At both the first and second nearest neighbor positions, the RDF of the structure under 8% strain along the [110] direction corresponds with that of the perfect orthorhombic crystal, suggesting a transfor-

mation from the γ-phase to the α''-phase. Therefore, applying tensile stress to γ-phase U–Mo alloys in various directions leads to different outcomes. Since α''-phase U–Mo alloys display poorer overall mechanical properties, tensile deformation should be conducted along the [100] direction in practical applications to prevent phase transformation and retain a γ-phase structure with superior mechanical properties.

5. Conclusion

The MD calculation method is utilized primarily to calculate the GSFE and GPFE curves of random solid solutions with three distinct compositions of γ-phase U–15 at.% Mo, U–20 at.% Mo, and U–25 at.% Mo. These calculations facilitate the determination of the preferential activation sequence of three slip systems and the competition between slip and twinning in γ-phase U-Mo alloys.

The preferential sequence of slip systems is determined by combining the GSFE curves with the modified P–N model to calculate the Peierls stress for the $\{110\}\langle 111\rangle$, $\{112\}\langle 111\rangle$, and $\{123\}\langle 111\rangle$ systems, yielding values of 478.99 MPa, 1065.82 MPa, and 1533.82 MPa, respectively. These findings suggest that the $\{110\}\langle 111\rangle$ slip system is the most easily activated. This conclusion is further supported by the analysis of misfit energy. It is verified that the calculated results for the $\{110\}\langle 111\rangle$ system align closely with experimental values. In light of the anisotropy observed during tensile tests, the Schmid factor is calculated, indicating that the $\{110\}\langle 111\rangle$ slip system is likely to be the first to activate under specific loading directions; however, this conclusion may change under varying material conditions.

To investigate the competition between slip and twinning in the $\{112\}\langle 111\rangle$ system of γ-phase U–Mo alloys, a comparison of the GSFE and GPFE curves reveals that the ratio of $\delta\gamma^{\text{twin}}/\delta\gamma^{\text{slip}}$ is less than 1 for all three compositions. Consequently, it is determined that twinning is likely to precede slipping in the $\{112\}\langle 111\rangle$ system under external loading. This conclusion is further validated through tensile tests conducted in the [100] direction. Additionally, tensile tests performed in the [110] direction demonstrate the γ-to-α'' phase transformation. Given that the α'' phase exhibits inferior overall mechanical properties, it is recommended that practical applications favor directions that promote twinning while inhibiting phase transformation during tensile testing.

Acknowledgment

Project supported by the National Natural Science Foundation of China (Grant No. 52271105).

References

[1] Kim Y S and Hofman G L 2011 *J. Nucl. Mater.* **419** 291
[2] Sinha V P, Hegde P V, Prasad G J, Dey G K and Kamath H S 2010 *J. Alloys Compd.* **506** 253
[3] Burkes D E, Fielding R S, Porter D L, Crawford D C and Meyer M K 2009 *J. Nucl. Mater.* **389** 458
[4] Neogy S, Saify M T, Jha S K, Srivastava D, Hussain M M, Dey G K and Singh R P 2012 *J. Nucl. Mater.* **422** 77
[5] Lopes D A, Restivo T A G and Padilha A F 2013 *J. Nucl. Mater.* **440** 304
[6] Meyer M K, Gan J, Jue J F, Keiser D D, Perez E, Robinson A, Wachs D M, Woolstenhulme N, Hofman G L and Kim Y S 2014 *Nucl. Eng. Technol.* **46** 169
[7] Kim Y S, Hofman G L, Yacout A M and Kim T K 2013 *J. Nucl. Mater.* **441** 520
[8] Kaity S, Banerjee J, Parida S C, Behere P G and Bhasin V 2020 *J. Nucl. Mater.* **532** 152046
[9] Morais N W S and Schön C G 2021 *J. Alloys Compd.* **871** 159501
[10] Park J M, Ryu H J, Lee G G, Kim H S, Lee Y S, Kim C K and Hofman G L 2006 *IAEA* **37** 45
[11] Eriksson N 2018 *Metall. Mater. Trans. A* **50** 72
[12] Hills R F, Butcher B R and Heywood J A 1961 *J. Less-Common Met.* **3** 155
[13] Woolum C 2014 Master's Thesis (Texas A & M University) p. 60
[14] Vatulin A V, Morozov A V, Suprun V B, Petrov Y I and Trifonov Y I 2004 *Met. Sci. Heat Treat.* **46** 484
[15] Kapoor R, Behera A N, Chakravartty J K and Hussain M M 2015 *Metall. Mater. Trans. A* **46** 251
[16] Grilli N, Tarleton E, Edmondson P D, Gussev M N and Cocks A C F 2020 *Phys. Rev. Mater.* **4** 043605
[17] Paidar V 1983 *Philos. Mag. A* **48** 231
[18] Kibey S, Liu J B, Johnson D D and Sehitoglu H 2007 *Acta. Mater.* **55** 6843
[19] Ostapovets A and Paidar V 2008 *Mater. Sci. Forum* **567–568** 69
[20] Ojha A, Sehitoglu H, Patriarca L and Maier H J 2014 *Model. Simul. Mater. Sc.* **22** 075010
[21] Kivshar Y S and Campbell D K 1993 *Phys. Rev. E* **48** 3077
[22] Ren Q, Joos B and Duesbery M S 1995 *Phys. Rev. B* **52** 13223
[23] Pellegrini Y P 2010 *Phys. Rev. B* **81** 024101
[24] Pan J S, Tong J M and Tian M B 1998 *Fundamentals of Materials Science* (Tsinghua University) p. 258
[25] Yu Z T 2021 Master's Thesis (Tsinghua University) p. 53
[26] Starikov S V, Kolotova L N, Kuksin A Y, Smirnova D E and Tseplyaev V I 2018 *J. Nucl. Mater.* **499** 451
[27] Jia J P, Huang H, Wang Z G, Zhang P C and Wu S 2013 *Rare Met. Mater. Eng.* **8** 4
[28] Li S Z, Ding X D, Deng J K, Lookman T, Li J, Ren X B, Sun J and Saxena A 2010 *Phys. Rev. B* **82** 205435
[29] Stukowski A 2010 *Model. Simul. Mater. Sc.* **18** 015012